Modeling Random Short Nano-/Micro-Fiber Reinforced Composites using the Extended Finite Element Method

Matthew G. Pike*and Caglar Oskay†

Department of Civil and Environmental Engineering
Vanderbilt University
Nashville, TN 37235

Abstract

This manuscript presents the formulation and implementation of an Extended Finite Element Method (XFEM) for random short fiber reinforced composite materials. A new enrichment function is proposed to incorporate the effect of random fiber inclusions within the XFEM framework to eliminate the need of using finite element meshes compliant with fiber inclusions. The motion of the fiber inclusions are modeled by constraining the deformation field along the domain of the fiber inclusions. Coupling the XFEM method along with the new enrichment function and constraint equations formulate the elastic response of short fiber reinforced composites. Numerical integration procedures are provided for accurate evaluation of the system response for fiber tips that lie on arbitrary positions within the problem domain. The performance of the proposed model is verified against the direct finite element method.

Keywords: Random short fiber composites, extended finite element, modeling, elastic properties

Introduction

Micro- and nano-fiber reinforced composites have been shown to exhibit good mechanical performance under static and dynamic loading conditions for a wide range of matrix materials

*Author address: VU Station B#351831, 2301 Vanderbilt Place, Nashville, TN 37235. Email: matthew.g.pike@vanderbilt.edu

†Corresponding author address: VU Station B#351831, 2301 Vanderbilt Place, Nashville, TN 37235. Email: caglar.oskay@vanderbilt.edu

and for a variety of engineering applications. A key advantage of these composites is that they can be tailored to perform optimally under a range of loading and environmental conditions. Fiber reinforcements provide additional unique properties including self sensing, self control of cracks and electromagnetic field shielding, making them attractive for multifunctional applications (Li 2003, Chung 2000, 2002, Reza et al. 2004, Fu and Chung 1996).

Modeling of the micro- and nano-fiber reinforced composite materials are traditionally conducted based on micromechanical modeling or through computational studies of representative volume elements (RVEs). The micromechanical modeling approaches are typically based on the Eshelby's solution of ellipsoidal inclusions embedded in a matrix in conjunction with Mori-Tanaka scheme (e.g., (Tandon and Weng 1986, Huang 2001, Bouaziz et al. 2007)), Hashin-Strichman bounds (Ponte-Castaneda and Willis 1995) and others. The ellipsoidal inclusions are taken to have a high aspect ratio to mimic the effect of the fiber geometries when such approaches are applied to model random fibers. The computational RVE modeling of the response of random fiber composites has also been proposed by a number of investigators (Bohm et al. 2002, Lusti et al. 2002). This approach is based on the 3-D resolution of the randomly generated fiber geometries, which becomes very challenging when the fiber aspect ratios are large due to the requirement to use very small elements in discretization of the fiber domains, and when large number of fibers are present to ensure mesh compatibility between the embedded fibers and the matrix.

The extended finite element method (XFEM) provides a way to eliminate the need to discretize the individual fibers and the compatibility requirements of the underlying discretization. The primary idea of the XFEM approach is to employ nodal enrichment functions, in addition to the standard finite element basis, capable of representing inhomogeneities and discontinuities within the problem domain rather than explicitly representing them through meshing (Moës et al. 1999). The local character of the base finite element formulation is kept by employing the partition of unity principle (Babuska and Melenk 1997). The discontinuities modeled by XFEM may be strong (i.e., displacement discontinuities) or weak (i.e., strain discontinuities). The strong discontinuity approach is suited to model cracks and fracture processes, whereas the weak discontinuities model internal boundaries such as holes and inclusions. XFEM approach has seen a rapid development in the past decade, which is summarized in Refs. (Mohammadi 2008, Belytschko et al. 2009). Sukumar et al. (2000) presented a methodology to model arbitrary holes and inclusions without remeshing the internal boundaries. The method couples the level set method with the XFEM method. Belytschko et al. (2001) proposed a technique for modeling arbitrary (including potentially intersecting) discontinuities in finite elements. The approximation for discontinuous elements uses the XFEM form and the surfaces of the discontinuities by the signed distance function. Chen et al. (2012) reviewed the treatment of tip, fully and partial enrichment of the finite elements and corresponding numerical integration techniques in the context of the XFEM approach. Hiriyur et al. (2011) proposed a methodology to incorporate the enrichments of multiple weakly discontinuous functions over a single element domain, removing the requirement of fine mesh resolution around interacting inclusions. Such important work of XFEM modeling has addressed inclusions that can be represented as a subdomain of the problem domain (e.g., spherical inclusions) or cracks. Modeling of short fibers with very high aspect ratios provide a somewhat different challenge, in which the discontinuity to be modeled is weak, yet assumed to occupy insignificant volume of the problem domain.

In this manuscript, we present the formulation and implementation of XFEM for random short fiber reinforced composite materials. A new enrichment function is proposed to incorporate the effect of random fiber inclusions within the XFEM framework to eliminate the need of using finite element meshes compliant with fiber inclusions. A key contribution of this work is to extend the XFEM for modeling weak discontinuities for inclusions that does not occupy volume. To this effect, the fibers are approximated as line discontinuities in a multi-dimensional domain. In the present work, the fibers are assumed to behave as a rigid body with no stretching or bending. The motion of the fiber inclusions are modeled by constraining the deformation field along the domain of the fiber inclusions. Coupling the XFEM method along with the new enrichment function and constraint equations formulate the elastic response of short fiber reinforced composites. Numerical integration procedures are provided for accurate evaluation of the system response for fiber tips that lie on arbitrary positions within the problem domain. The performance of the proposed model is verified against the direct finite element method. The formulation presented in this study is for multiple dimensions but the numerical aspects and examples focus on the two-dimensional problems.

The remainder of this manuscript is organized as follows. In Section 2, the fundamental concepts of the XFEM method is introduced and discussed. In Section 3, the application of the XFEM method to short fiber reinforced composite materials. The fiber inclusion enrichment function and constraints to define fiber motion is described. Section 4 provides the governing equations, the numerical formulation of the XFEM method for short fiber reinforced composites and the treatment of partially enriched elements. The assessment of the performance of the proposed approach is presented in Section 5. Conclusions and future research directions in this area are discussed in Section 6.

The Extended Finite Element Method

The extended finite element method (XFEM) is based on the expression of the response field using the following approximation:

$$\mathbf{u}(\mathbf{x}) = \sum_{a=1}^{n_n} N_a(\mathbf{x})\hat{\mathbf{u}}_a + \sum_{b \in \mathcal{I}} N_b(\mathbf{x})\psi(\mathbf{x})\hat{\mathbf{c}}_b \tag{1}$$

in which, $\mathbf{u}$ denotes displacements; N_a the finite element shape function associated with node a; a and b the dummy indices of summation over all nodes and enriched nodes respectively; ψ an enrichment function; $\hat{\mathbf{u}}_a$ and $\hat{\mathbf{c}}_b$ the nodal coefficients of the standard and enrichment shape functions, respectively; n_n the total number of mesh nodes in a finite element discretization; and $\mathcal{I}$ is an index set of enriched nodes. The first right hand side term of Eq. 1 corresponds to the standard finite element approximation of the response field, whereas the second part is the enrichment to the approximation space based on a predefined enrichment function, ψ. The enrichment function is known a-priori to represent the response well within the whole domain or a subdomain of the problem, such as around strong or weak discontinuities. The index set, $\mathcal{I}$ reflects the extent to which the domain of the problem is enriched.

The foundation of XFEM is the partition of unity method (PUM) formalized by Babuska and Melenk (1997), which provides the foundation of the enrichment approximation in Eq. 1. In PUM, the enrichment is computed as a product of the enrichment function and shape functions that satisfy the partition of unity property. The standard Lagrangian finite element shape functions are well suited for this purpose as they satisfy the partition of unity property. An advantage of using Eq. 1 is that the resulting system of discrete equations is sparse.

Modeling Embedded Short Fibers

This section presents the XFEM enrichment functions that will be employed in modeling the deformation response of short fibers embedded in a matrix. The short fibers are modeled as one-dimensional rods in view of their very high aspect ratios. The displacement of the fibers within the problem domain under loading is enforced through constraint equations described in Section 3.2.

Enrichment function

We seek to develop an enrichment function for the short fiber inclusions. This is achieved through defining level set functions for the fiber domain and the fiber tips separately. In a fiber reinforced composite, there exists a multitude of fibers each of which much be represented using a separate enrichment function. For the simplicity of the presentation, we consider a single inclusion to derive the enrichment function. The application of the enrichment function to address the multiple fibers is straightforward provided that no overlapping occurs. The overlapping refers to the presence of multiple fibers within a single finite element as opposed to overlapping of the fiber domains, which is nonphysical and avoided.

Let $\Omega \subset \mathbb{R}^d$ be the open bounded domain of the composite body, where $d = 2, 3$ is the number of space dimensions. The reinforcing fibers are entirely embedded in Ω, and are taken to be straight with very high aspect ratio compared to the overall size of the composite body. The domain of a single fiber is therefore approximated by a line segment, parameterized by s, such that:

$$\mathbf{x} = \mathbf{x}_c + \frac{\mathbf{x}_2 - \mathbf{x}_1}{2} s; \quad -1 \leq s \leq 1; \quad \mathbf{x} \in \Gamma \tag{2}$$

where, $\mathbf{x}_1$ and $\mathbf{x}_2$ denote the positions of the fiber tips, and $\mathbf{x}_c$ the position of the center of the fiber (i.e., $\mathbf{x}_c = (\mathbf{x}_1 + \mathbf{x}_2)/2$). The level set functions associated with the fiber tips are expressed as:

$$\phi_\alpha(\mathbf{x}) = (\mathbf{x} - \mathbf{x}_\alpha) \cdot \mathbf{t}_\alpha; \quad \alpha = 1, 2 \tag{3}$$

in which, $\mathbf{t}_\alpha$ denotes the tangent at the corresponding fiber tip (i.e., $\mathbf{t}_1 = (\mathbf{x}_1 - \mathbf{x}_2)/l$ and $\mathbf{t}_2 = (\mathbf{x}_2 - \mathbf{x}_1)/l = -\mathbf{t}_1$). $l = \|\mathbf{x}_2 - \mathbf{x}_1\|$ denotes the length of the fiber. Figure 2 illustrates the level set functions associated with the fiber tips. ϕ_α provides the zero level set along the plane normal to the fiber passing through the fiber tip. The value of ϕ_α is positive on the outer part of the domain cut by the zero level set, and negative elsewhere within the composite body. A third level set is defined as:

$$\phi_c(\mathbf{x}) = \|\mathbf{x} - \mathcal{P}(\mathbf{x})\| \tag{4}$$

in which, $\mathcal{P}(\mathbf{x})$ is the projection of $\mathbf{x}$ onto the fiber:

$$\mathcal{P}(\mathbf{x}) = \mathbf{x}_1 + [(\mathbf{x} - \mathbf{x}_1) \cdot \mathbf{t}_2]\,\mathbf{t}_2 = \mathbf{x}_2 + [(\mathbf{x} - \mathbf{x}_2) \cdot \mathbf{t}_1]\,\mathbf{t}_1 \tag{5}$$

ϕ_c is the level set function associated with domain of the fiber. ϕ_c divides the domain of the body along the plane of the fiber with positive values on each side and zero along the fiber as shown in Fig. 2. Employing Eqs. 3 and 4, the enrichment function for the fiber is written as:

$$\psi(\mathbf{x}) = \left[\prod_{\alpha=1}^{2} H(-\phi_\alpha)\right] \phi_c(\mathbf{x}) + \sum_{\alpha=1}^{2} H(\phi_\alpha) d_\alpha(\mathbf{x}) \tag{6}$$

with,

$$H(f) = \begin{cases} 1 & f \geq 0 \\ 0 & f < 0 \end{cases} \tag{7}$$

and $d_\alpha(\mathbf{x}) = \|\mathbf{x} - \mathbf{x}_\alpha\|$ denotes the distance function to the fiber tip, α. The enrichment function expressed in Eq. 6 has the form of the V-shaped enrichment functions employed in inclusion problems (Moës et al. 2003), with caps defined at the tips of the fiber. Adding $\psi(\mathbf{x})$ to the approximation basis of the solution field introduces a strain discontinuity mode along the position of the fiber. The displacements around the fiber can therefore be accurately captured without explicitly discretizing the fiber domain. The particular form chosen for $\psi(\mathbf{x})$ (Eq. 6) ensures that approximation basis captures the strain discontinuity but stay smooth otherwise around the tip and sides of the fiber. Three dimensional and planar views of the enrichment function are illustrated in Fig. 3 a-b. The enrichment functions around a fiber tip multiplied by the finite element shape functions of a quadrilateral element are illustrated in Fig. 4.

The enrichment function in Eq. 6 is nonzero everywhere in the composite domain except on the fiber. The direct application of this enrichment function therefore leads to the enrichment of all nodes within the domain. This is undesirable since away from the fiber, the enrichment does not enlarge the trial space spanned by the standard finite element shape functions, yet increase the size of the linear system. This is circumvented by considering the enrichment of a small subdomain around the fiber, while employing standard finite element shape functions in the remainder of the problem domain. By this approach, the domain of the composite is taken to consist of four regions as illustrated in Fig. 5: (1) Far field elements with no enrichment; (2) elements with partial enrichment; (3) fully enriched elements crossed by the fiber; and (4) fully enriched elements partially crossed by the fiber that contain the fiber tip. The support of the enrichment region is provided by the sides (or faces) of the partially enriched elements formed by their standard nodes. The numerical treatment of the regions are different from each other and described in Section . As illustrated in Fig. 5, the enrichment domain is chosen based on the discretization as opposed to the geometry of the problem domain that is typically used in crack modeling with XFEM (e.g., crack tip enrichment defined within a specified radius from the crack tip). Since the fiber tip enrichment functions employed in this study are not defined based on geometry and smoothly vary (similar to the Heaviside enrichments employed on the sides of the fibers or crack faces), geometry based enrichment domain selection is not critical to the method performance.

Rigid fiber constraints

The enrichment function provides the necessary weak (i.e., strain) discontinuity within a finite element to describe the effect of inclusion on the response of the matrix around it, but does not incorporate the kinematics of the fiber itself. The deformation of the fiber inclusion is typically a function of the stiffness contrast between the fiber and the matrix, flexural rigidity and the length of the fiber. For relatively short fibers embedded in matrix of significantly lower stiffness, the bending and stretching of the fiber are small. Early works indicate a relative insensitivity of the overall composite stiffness to constituent stiffness ratio, particularly at high values (Russel 1973). In this manuscript, the fibers are idealized as rigid bodies going through only translation and rotation but no bending and stretching. This condition may be imposed by considering the following constraint:

$$\mathbf{g}(\mathbf{x}) := \mathbf{u}(\mathbf{x}) - \mathbf{u}_c - (\mathbf{R} - \boldsymbol{\delta}) \cdot (\mathbf{x} - \mathbf{x}_c) = \mathbf{0}; \quad \mathbf{x} \in \Gamma \tag{8}$$

in which, $\mathbf{u}_c$ is a constant vector of translation, $\mathbf{R}$ the orthogonal tensor of rigid body rotation about the center of the fiber; and $\boldsymbol{\delta}$ the Kronecker Delta. The orthogonal transformation imposed by the rigid body rotation constraint is valid for large rotations, but is a nonlinear constraint. Assuming the rotation of the rigid fiber supported by the matrix remains small, Eq. 8 is rewritten using a linear constraint equation as:

$$\mathbf{g}(\mathbf{x}) := \mathbf{u}(\mathbf{x}) - \mathbf{u}_c - \frac{l}{2} s\left(\mathbf{x}\right)\theta\mathbf{n} = \mathbf{0}; \quad \mathbf{x} \in \Gamma \tag{9}$$

where, θ is the angle of rotation, and $\mathbf{n}$ the normal to the fiber direction as illustrated in Fig. 1c. Equation 9 implies that the rotational component of the fiber deformation is normal to the original fiber orientation, which is valid for small θ.

Governing Equations and Formulation

The governing equations for the deformation response of the short fiber reinforced composite is:

$$\nabla \cdot \boldsymbol{\sigma}\left(\mathbf{x}\right) = \mathbf{0}; \quad \mathbf{x} \in \Omega \tag{10}$$

$$\boldsymbol{\sigma}\left(\mathbf{x}\right) = \mathbf{L} : \boldsymbol{\epsilon}\left(\mathbf{x}\right) = \mathbf{L} : \nabla^s \mathbf{u}\left(\mathbf{x}\right); \quad \mathbf{x} \in \Omega \tag{11}$$

where, σ is the stress tensor; ϵ the strain tensor given as the symmetric gradient of the displacement field, $\mathbf{u}$; and $\mathbf{L}$ is the tensor of elastic moduli of the matrix material. $\mathbf{L}$ is taken to be a symmetric and strongly elliptic fourth order tensor. The boundary conditions of the deformation problem are:

$$\mathbf{u}\left(\mathbf{x}\right) = \tilde{\mathbf{u}}\left(\mathbf{x}\right); \quad \mathbf{x} \in \partial\Omega_u \tag{12}$$

$$\boldsymbol{\sigma}\left(\mathbf{x}\right) \cdot \mathbf{n}\left(\mathbf{x}\right) = \tilde{\mathbf{t}}\left(\mathbf{x}\right); \quad \mathbf{x} \in \partial\Omega_t \tag{13}$$

in which, $\tilde{\mathbf{u}}$ and $\tilde{\mathbf{t}}$ are the prescribed boundary displacement and tractions, respectively. $\partial\Omega_u$ and $\partial\Omega_t$ are the non-overlapping essential and natural exterior boundary parts such that $\partial\Omega_u \cup \partial\Omega_t = \partial\Omega$. The domain of the composite body includes n_f straight fibers with varying length and orientations. Neglecting the bending and stretching of the fibers and assuming small rotations of the fibers, the following constraint equations are imposed on the displacement response of the composite:

$$\mathbf{u}(\mathbf{x}) = \mathbf{u}_c^i + \frac{l}{2} s^i\left(\mathbf{x}\right)\theta^i\mathbf{n}^i; \quad \mathbf{x} \in \Gamma^i; \quad i = 1, 2, \ldots, n_f \tag{14}$$

Superscript i, indicates i^{th} fiber.

XFEM formulation

The extended finite element method is employed to discretize and evaluate the governing equations (Eqs. 10-14). Using the standard Ritz-Galerkin procedure and employing the penalty function formulation for imposing the constraints, the problem can be posed in the weak form as: Given the boundary data and the matrix elastic moduli matrix, find $\mathbf{u} \in \mathcal{U}_{\tilde{\mathbf{u}}}$ such that for all $\boldsymbol{\nu} \in \mathcal{U}_{\mathbf{0}}$

$$\int_{\Omega} \nabla \boldsymbol{\nu} : \mathbf{L} : \nabla \mathbf{u} \, d\Omega + \sum_{i=1}^{n_f} \int_{\Gamma^i} \gamma \boldsymbol{\nu} \cdot \mathbf{g}^i \, d\Gamma = \int_{\partial\Omega_t} \boldsymbol{\nu} \cdot \tilde{\mathbf{t}} \, d\Gamma \tag{15}$$

$\mathbf{g}^i$ is the displacement constraint for fiber, i; γ the penalty parameter chosen sufficiently large to ensure enforcement of the constraint equations. The appropriate spaces for the trial and test functions are:

$$\mathcal{U}_{\mathbf{v}} := \left\{ \mathbf{u} \in [H^1(\Omega)]^d \;\middle|\; \mathbf{u} = \mathbf{v} \text{ on } \mathbf{x} \in \partial\Omega_u \right\} \tag{16}$$

where, $H^1(\Omega)$ is the Sobolev space of functions with square integrable values and derivatives defined on the problem domain. The subscript $\mathbf{v}$ is equal to $\tilde{\mathbf{u}}$ (i.e., the prescribed boundary data) in the case of the trial function and equal to zero in the case of the test function.

The discretization of the trial and test functions follows the Galerkin method based on Eq. 1. We start by the decomposition of the problem domain into finite elements. In contrast to the standard finite element approach, the mesh does not necessarily conform to the fiber domains, i.e., fibers are allowed to lie within the element domains. The first term in Eq. 15 is then expressed as:

$$\int_{\Omega} \nabla \boldsymbol{\nu} : \mathbf{L} : \nabla \mathbf{u} \, d\Omega = \sum_{e=1}^{n_e} \int_{\Omega_e} \nabla \boldsymbol{\nu} : \mathbf{L} : \nabla \mathbf{u} \, d\Omega \tag{17}$$

in which, n_e is the total number of elements; and Ω_e the domain of the element, e. Substituting Eq. 1 into Eq. 17 and switching to the Voigt notation with contracted indices for simplicity, the element level integral is expressed as:

$$\int_{\Omega_e} \nabla \boldsymbol{\nu} : \mathbf{L} : \nabla \mathbf{u} \, d\Omega = (\mathbf{V}^e)^T \int_{\Omega_e} (\mathbf{B}^e)^T \mathbf{L} \, \mathbf{B}^e \, d\Omega \, \mathbf{U}^e = (\mathbf{V}^e)^T \mathbf{K}^e \mathbf{U}^e \tag{18}$$

in which, superscript T denotes the transpose operator; and $\mathbf{U}^e$ and $\mathbf{V}^e$ denote the vectors of nodal coefficients of the trial and test functions in element, e:

$$\mathbf{U}^e = \left\{ (\hat{\mathbf{u}}_1^e)^T (\hat{\mathbf{u}}_2^e)^T \dots (\hat{\mathbf{u}}_{n_n^e}^e)^T (\hat{\mathbf{c}}_{I_1^e}^e)^T (\hat{\mathbf{c}}_{I_2^e}^e)^T \dots (\hat{\mathbf{c}}_{I_{n_{en}^e}^e}^e)^T \right\}^T \tag{19}$$

where, $\hat{\mathbf{u}}_a^e$ and $\hat{\mathbf{c}}_a^e$ denote the vectors of unknown coefficients for standard and extended degrees of freedom within the element, e at node a; and I^e is the index set of nodes that are enriched within the element. I^e an empty set indicates a standard finite element; I^e that consists of all nodes within the element indicates full enrichment of the element, whereas I^e that consists of a subset of nodes indicates partial enrichment. $\mathbf{B}^e$ corresponds to the gradient operation expressed as:

$$\mathbf{B}^e = \left\{ \hat{\mathbf{B}}_1^e \;\; \hat{\mathbf{B}}_2^e \dots \hat{\mathbf{B}}_{n_n^e}^e \;\; \bar{\mathbf{B}}_{I_1^e}^e \;\; \bar{\mathbf{B}}_{I_2^e}^e \dots \bar{\mathbf{B}}_{I_{n_{en}^e}}^e \right\} \tag{20}$$

in which,

$$\hat{\mathbf{B}}_a^e = \begin{bmatrix} N_{a,x}^e & 0 \\ 0 & N_{a,y}^e \\ N_{a,y}^e & N_{a,x}^e \end{bmatrix} \text{(2-D)} \quad \hat{\mathbf{B}}_a^e = \begin{bmatrix} N_{a,x}^e & 0 & 0 & N_{a,y}^e & 0 & N_{a,z}^e \\ 0 & N_{a,y}^e & 0 & N_{a,x}^e & N_{a,z}^e & 0 \\ 0 & 0 & N_{a,z}^e & 0 & N_{a,y}^e & N_{a,x}^e \end{bmatrix}^T \text{(3-D)} \tag{21}$$

where, a subscript followed by a comma indicates differentiation. For the enrichment degrees of freedom, the gradient operation takes the form:

$$\bar{\mathbf{B}}_a^e(\mathbf{x}) = \hat{\mathbf{B}}_a^e(\mathbf{x})\,\psi(\mathbf{x}) + \tilde{\mathbf{B}}_a^e(\mathbf{x}) \tag{22}$$

$$\tilde{\mathbf{B}}_a^e = \begin{bmatrix} \psi_{,x} & 0 \\ 0 & \psi_{,y} \\ \psi_{,y} & \psi_{,x} \end{bmatrix} N_a^e \text{ (2-D)} \quad \tilde{\mathbf{B}}_a^e = \begin{bmatrix} \psi_{,x} & 0 & 0 & \psi_{,y} & 0 & \psi_{,z} \\ 0 & \psi_{,y} & 0 & \psi_{,x} & \psi_{,z} & 0 \\ 0 & 0 & \psi_{,z} & 0 & \psi_{,y} & \psi_{,x} \end{bmatrix}^T N_a^e \text{ (3-D)} \tag{23}$$

The formulation of the third term in Eq. 15 proceeds similarly. Decomposing the boundary integral into its elemental components yields:

$$\int_{\partial\Omega_t} \boldsymbol{\nu} \cdot \tilde{\mathbf{t}}\, d\Gamma = \sum_{e \in I_t} \int_{\partial\Omega_t} \boldsymbol{\nu} \cdot \tilde{\mathbf{t}}\, d\Gamma \tag{24}$$

in which, I_t denotes the index set of elements at the boundary $\partial\Omega_t$. Substituting Eq. 1 into

Eq. 24, the element level boundary integral is expressed as:

$$\int_{\partial\Omega_t} \boldsymbol{\nu} \cdot \tilde{\mathbf{t}}\, d\Gamma = (\mathbf{V}^e)^T \int_{\partial\Omega_t} \mathbf{f}^e(\mathbf{x})\, d\Gamma = (\mathbf{V}^e)^T \mathbf{F}^e \tag{25}$$

where,

$$\mathbf{f}^e = \left\{ (\hat{\mathbf{f}}_1^e)^T (\hat{\mathbf{f}}_2^e)^T \dots (\hat{\mathbf{f}}_{n_n^e}^e)^T (\tilde{\mathbf{f}}_{I_1^e}^e)^T (\tilde{\mathbf{f}}_{I_2^e}^e)^T \dots (\tilde{\mathbf{f}}_{I_{n_{en}^e}^e}^e)^T \right\}^T \tag{26}$$

The components of the element force vector are:

$$\hat{\mathbf{f}}_a^e(\mathbf{x}) = N_a^e(\mathbf{x})\, \tilde{\mathbf{t}}(\mathbf{x})\,; \quad \tilde{\mathbf{f}}_a^e(\mathbf{x}) = \hat{\mathbf{f}}_a^e(\mathbf{x})\, \psi(\mathbf{x}) \tag{27}$$

Defining the global vector of unknown nodal coefficients as:

$$\mathbf{U} = \left\{ (\hat{\mathbf{u}}_1)^T (\hat{\mathbf{u}}_2)^T \dots (\hat{\mathbf{u}}_{n_n})^T (\hat{\mathbf{c}}_{I_1})^T (\hat{\mathbf{c}}_{I_2})^T \dots (\hat{\mathbf{c}}_{I_{n_{en}}})^T \right\}^T \tag{28}$$

The global stiffness matrix, $\hat{\mathbf{K}}$ and the force vectors are obtained by assembling the corresponding element matrices (i.e., $\mathbf{K}^e$ and $\mathbf{F}^e$):

$$\hat{\mathbf{K}} = \mathop{\mathbf{A}}_{e=1}^{n_e} \mathbf{K}^e; \quad \mathbf{F} = \mathop{\mathbf{A}}_{e=1}^{n_e} \mathbf{F}^e; \tag{29}$$

Constraint equations

The constraint equation for the i^{th} fiber ($\mathbf{g}^i$) indicates that the motion of the fiber is fully defined by a translation vector and a rotation angle. These unknowns are interpreted as the translation of the fiber midpoint (i.e., $\mathbf{u}_c^i$) and the rotation angle of the fiber about the fiber midpoint (i.e., θ^i). The translation vector is obtained as a function of the displacement field by integrating the constraint equation over the domain of the fiber and normalizing with the fiber length:

$$\frac{1}{l^i} \int_{\Gamma^i} \mathbf{g}^i(\mathbf{x})\, d\Gamma = \frac{1}{l^i} \int_{\Gamma^i} \mathbf{u}(\mathbf{x})\, d\Gamma - \mathbf{u}_c^i - \frac{\theta^i}{2} \int_{\Gamma^i} s(\mathbf{x})\, d\Gamma \mathbf{n}^i = \mathbf{0} \tag{30}$$

Observing that the rotation term vanishes, the translation vector reads:

$$\mathbf{u}_c^i = \frac{1}{l^i} \int_{\Gamma^i} \mathbf{u}(\mathbf{x})\, d\Gamma \tag{31}$$

The rotation angle is obtained by taking the inner product of the constraint equation with the fiber normal, $\mathbf{n}^i$ and averaging over the domain of the fiber:

$$\theta = \frac{2}{(l^i)^2} \int_{\Gamma^i} \frac{\mathbf{u}(\mathbf{x}) \cdot \mathbf{n}^i}{s(\mathbf{x})} d\Gamma \tag{32}$$

The constraint equation for fiber, i becomes:

$$\mathbf{g}^i(\mathbf{x}) = \mathbf{u}(\mathbf{x}) - \frac{1}{l^i} \int_{\Gamma^i} \mathbf{u}(\mathbf{x})\, d\Gamma - \frac{1}{l^i} s(\mathbf{x}) \int_{\Gamma^i} \frac{\mathbf{u}(\mathbf{x}) \cdot \mathbf{n}^i}{s(\mathbf{x})} d\Gamma\, \mathbf{n}^i \tag{33}$$

The enrichment function ψ vanishes within the fiber domain due to the zero level set functions as illustrated in Fig. 3. Therefore only the the standard shape functions are employed in the discretization of the displacement field along the fiber domain and the enrichment function does not affect the imposition of the constraint. Substituting Eq. 33 into Eq. 15 and decomposing the integral into element contributions, the first term of the constraint equation is written as:

$$\int_{\Gamma^i} \gamma \boldsymbol{\nu}(\mathbf{x}) \cdot \mathbf{u}(\mathbf{x})\; d\Gamma = \sum_{e \in I^i} \int_{\Gamma^i_e} \gamma \boldsymbol{\nu}(\mathbf{x}) \cdot \mathbf{u}(\mathbf{x})\; d\Gamma \tag{34}$$

where, I^i is the index set of all fully enriched elements crossed by the fiber, i. The element level integration is expressed in the vector form as follows:

$$\int_{\Gamma^i_e} \gamma \boldsymbol{\nu}(\mathbf{x}) \cdot \mathbf{u}(\mathbf{x})\; d\Gamma = (\mathbf{V}^e)^T \int_{\Gamma^i_e} \gamma (\hat{\mathbf{N}}^e)^T \hat{\mathbf{N}}^e d\Gamma\, \mathbf{U}^e = (\mathbf{V}^e)^T \mathbf{K}^{ei}_{c1} \mathbf{U}^e \tag{35}$$

where,

$$\hat{\mathbf{N}}^e(\mathbf{x}) = \left\{ N^e_1 \boldsymbol{\delta}\; N^e_2 \boldsymbol{\delta} \ldots N^e_{n^e_n} \boldsymbol{\delta} \right\}^T \tag{36}$$

$\boldsymbol{\delta}$ is the Kronecker delta. The contribution of the first term of the penalty function to the global system of equations can be computed using the standard assembly operation:

$$\hat{\mathbf{K}}^i_{c1} = \mathop{\mathbf{A}}_{e=1}^{n_e} \mathbf{K}^{ei}_{c1} \tag{37}$$

The second and the third terms of the constraint equation take the following form when expressed in terms of the element components, respectively:

$$\frac{\gamma}{l^i}\int_{\Gamma^i}\boldsymbol{\nu}\left(\mathbf{x}\right)d\Gamma\cdot\int_{\Gamma^i}\mathbf{u}\left(\mathbf{x}\right)d\Gamma=\frac{\gamma}{l^i}\sum_{e\in I^i}\int_{\Gamma^i_e}\boldsymbol{\nu}\left(\mathbf{x}\right)d\Gamma\cdot\sum_{e'\in I^i}\int_{\Gamma^i_{e'}}\mathbf{u}\left(\mathbf{x}\right)d\Gamma \tag{38}$$

$$\frac{\gamma}{l^i}\int_{\Gamma^i}s\left(\mathbf{x}\right)\boldsymbol{\nu}\cdot\mathbf{n}^i d\Gamma\int_{\Gamma^i}\frac{\mathbf{u}\cdot\mathbf{n}^i}{s\left(\mathbf{x}\right)}d\Gamma=\frac{\gamma}{l^i}\sum_{e\in I^i}\int_{\Gamma^i_e}s\left(\mathbf{x}\right)\boldsymbol{\nu}\cdot\mathbf{n}^i d\Gamma\sum_{e'\in I^i}\int_{\Gamma^i_{e'}}\frac{\mathbf{u}\cdot\mathbf{n}^i}{s\left(\mathbf{x}\right)}d\Gamma \tag{39}$$

The elemental components of the above equations are expressed in the vector form as:

$$\int_{\Gamma^i_e}\boldsymbol{\nu}d\Gamma=(\mathbf{V}^e)^T\int_{\Gamma^i_e}(\hat{\mathbf{N}}^e)^T d\Gamma=(\mathbf{V}^e)^T(\tilde{\mathbf{N}}^e)^T;\quad\int_{\Gamma^i_e}\mathbf{u}d\Gamma=\tilde{\mathbf{N}}^e\mathbf{U}^e \tag{40}$$

$$\int_{\Gamma^i_e}s\boldsymbol{\nu}\cdot\mathbf{n}^i d\Gamma=(\mathbf{V}^e)^T(\tilde{\mathbf{M}}^e_1)^T;\quad\int_{\Gamma^i_e}\frac{\mathbf{u}\cdot\mathbf{n}^i}{s\left(\mathbf{x}\right)}d\Gamma=\tilde{\mathbf{M}}^e_2\mathbf{U}^e \tag{41}$$

where,

$$\tilde{\mathbf{M}}^e_1=\int_{\Gamma^i_e}s\left(\mathbf{x}\right)\hat{\mathbf{N}}^e\left(\mathbf{x}\right)\mathbf{n}^i d\Gamma;\quad\tilde{\mathbf{M}}^e_1=\int_{\Gamma^i_e}\frac{\hat{\mathbf{N}}^e\left(\mathbf{x}\right)\mathbf{n}^i}{s\left(\mathbf{x}\right)}d\Gamma \tag{42}$$

The contributions of the second and third terms of the constraint equation to the global equation system is computed by assembling $\tilde{\mathbf{N}}^e$, $\tilde{\mathbf{M}}^e_1$ and $\tilde{\mathbf{M}}^e_2$. The contribution to the stiffness matrix is:

$$\hat{\mathbf{K}}^i_{c2}=\frac{\gamma}{l^i}\left[(\tilde{\mathbf{N}})^T\tilde{\mathbf{N}}+(\tilde{\mathbf{M}}_1)^T\tilde{\mathbf{M}}_2\right] \tag{43}$$

in which, $\tilde{\mathbf{N}}$, $\tilde{\mathbf{M}}_1$ and $\tilde{\mathbf{M}}_2$ are assembled from the element counterparts through the standard assembly operations. The final system of equations to be evaluated for unknown nodal coefficients is:

$$\mathbf{K}\mathbf{U}=\mathbf{F};\quad\mathbf{K}=\hat{\mathbf{K}}+\sum_{i=1}^{n_f}\left[\hat{\mathbf{K}}^i_{c1}-\hat{\mathbf{K}}^i_{c2}\right] \tag{44}$$

Numerical integration

To be able to compute the linear system of Eq. 44, it is necessary to numerically compute the element level integrals for $\mathbf{K}^e$, $\mathbf{F}^e$, $\mathbf{K}^{ei}_{c1}$, $\mathbf{K}^{ei}_{c2}$, $\tilde{\mathbf{N}}^{ei}$, $\tilde{\mathbf{M}}^{ei}_1$ and $\tilde{\mathbf{M}}^{ei}_2$ as defined in the previous section. The integration rules employed in the standard finite element method is not sufficient since the higher order functions (i.e., enrichment functions) need to be integrated. The integration rules are defined for all possible cases of fiber positions. While the general treatment of the numerical integration can be generalized to 3-D without conceptual difficulty, the current discussion focuses on the 2-D cases. The possible cases of fiber positions as illustrated in Fig. 6

are:

1. Far field elements with no enrichment: Standard integration orders apply since no additional functions are employed in these elements.

2. Partially enriched elements: Integration rules with elevated order are employed since some of the nodes include enrichment functions.

3. Fully enriched elements entirely crossed by the fiber: The elements are split by the fiber. Each part is further decomposed into triangular sub-elements using Delaunay triangulation and higher order integration rules are used to capture high order enrichment fields within each sub-element.

4. Fully enriched elements that contain fiber tips: The elements are split along the normal direction at the fiber tip, as well as along the fiber direction. Each part formed by the split is further decomposed into triangular sub-elements using Delaunay triangulation and higher order integration rules are used to capture high order enrichment fields within each sub-element. The splitting based on the fiber normal ensures that the components of the enrichment function that pertain to the fiber tip and fiber level sets are integrated separately.

Typical integration schemes employed in fully enriched elements are shown in Fig. 6. In full enrichment cases, triangular sub-elements aligned with the fiber faces are used in the integration of a 2-D quadrilateral. The triangular sub-elements contain three integration points and use the standard Gauss quadrature rules. In the partially enriched elements and the far-field elements, Gauss quadrature rule with 4 integration points is performed (Chen et al. 2012). The partially enriched elements do not have sub elements since the fiber does not cross through the element.

The line integration of the i^{th} constraint equation is performed on the domain of the i^{th} fiber based on the Gauss quadrature. The rule employed in the integration of the constraint equation has a significant influence on the accuracy characteristics of the model, similar to the sensitivity of accuracy with respect to the integration of the enrichment functions, reported previously (e.g., (Bordas et al. 2010)). The number of integration points along the fiber (n_g^i) is determined using a heuristic formula, as a function of the fiber length (l^i) and the mesh density (h) given as:

$$n_g^i = \lfloor\lfloor \frac{1.3 l^i}{h} \rceil\rceil_{\mathrm{e}} \tag{45}$$

where, $\lfloor\lfloor \cdot \rceil\rceil_{\mathrm{e}}$ indicates approximation to the nearest even integer. Only even number of integration points are used to ensure that the no gauss point lies on the fiber center, since this causes the rotation constraint (i.e., Eq. 39) to tend to infinity. When more than 12 integration points are needed in the constraint equation, the domain of integration is split and the integration is performed separately for each split part such that the quadrature formulas per split fiber part does not exceed 12 integration points. If a fiber crosses an element for a very small fraction of the fiber length, it is possible to have no integration points within the element despite the presence of the fiber within the element.

Treatment of Partially Enriched Elements

It has been previously shown that the treatment of the partially enriched elements has an effect on the accuracy and convergence of XFEM models (Fries 2008). This is because within partially enriched elements (a) the partition of unity property no longer holds and (b) the affine transformations (e.g. constant strain modes) cannot be represented exactly. A number of solution strategies exist to alleviate these problems (e.g. Chessa et al. (2003), Laborde et al. (2005)). One method involves the modification of the enrichment using a ramp function that has a local support within the partially enriched element and enriching all nodes of the partially enriched element using the modified enrichment function (Fries 2008). In the current study a similar modification of the enrichment function is considered. Let $\hat{\psi}(\mathbf{x})$ denote the modified enrichment function within a partially enriched finite element:

$$\hat{\psi}(\mathbf{x}) = \sum_{c \in \mathcal{I}_e} N_c(\mathbf{x}) \psi(\mathbf{x}); \quad \mathbf{x} \in \Omega_e \tag{46}$$

where, $\mathcal{I}_e$ are the nodes in the partially enriched element, Ω_e, that are connected to fully enriched elements. The modified enrichment function is active at all nodes of the partially enriched element:

$$\mathbf{u}^e(\mathbf{x}) = \sum_{a=1}^{n_n^e} N_a^e(\mathbf{x}) \hat{\mathbf{u}}_a^e + \sum_{a=1}^{n_n^e} N_a^e(\mathbf{x}) \hat{\psi}(\mathbf{x}) \hat{\mathbf{c}}_a^e \tag{47}$$

in which, superscript e indicates that all pertinent variables are defined in the partially enriched element, e. The modifications needed in the finite element implementation discussed above is to use the modified enrichment functions (instead of the enrichment functions) and considering enrichment of all nodes within the partially enriched elements.

Numerical Examples

In this section we present two numerical examples to demonstrate the performance of the proposed XFEM model in evaluating the response of short fiber reinforced composites in two-dimensional setting. The first example illustrates the accuracy characteristics of the method using a single fiber inclusion embedded in a matrix, whereas the second example considers multiple random short fibers embedded in a matrix.

Single fiber inclusion

The XFEM formulation is verified against the standard finite element method using a composite enriched with a single fiber. The schematic representation of the model problem is shown in Fig. 7. The size of the domain is 5mm by 5mm and the fiber size is approximately 1mm. The domain is subjected to uniform uniaxial tensile loading applied at the right edge. The fiber is placed such that a non-uniform deformation and stress distribution is achieved within the matrix. The Young's Modulus and Poisson's ratio of the matrix material are 14 GPa and 0.3, respectively. The reference model consists of a very densely meshed finite element model in which the fiber is enforced to undergo rigid body motion. The rigid fiber motion in the reference model is prescribed by constraining nodal degrees of freedom that lay along the fiber domain using the multi point constraint method. Similar to the XFEM approach, the fiber is idealized as a line segment. Reference simulation discretizations ranging from 400 elements up to approximately 625,000 elements have been studied to ensure mesh convergence. The simulations confirmed that the response is very accurately captured at such high levels of discretization. All reported reference simulation results are based on approximately 625,000-element discretizations.

Figure 8 shows the accuracy of the XFEM model compared to the reference simulation. The accuracy is assessed at four different locations as illustrated in Fig. 7. Points A, B, C, D refer to the left fiber tip, right fiber tip, top right corner and bottom right corner within the problem domain, respectively. In Fig. 8, the point-wise errors are computed using the L2 norm and plotted against the normalized mesh density (h/l). The reference simulation considers a very fine and nonuniform grid (to conform to the fiber domain). The discretization of the XFEM model is a square and uniform grid. In these simulations, the fiber tip locations for all element sizes always coincide with a node. The error for the corner nodes reduces monotonically with increasing mesh density. Errors at the fiber tips displayed slight variations in accuracy as a function of mesh density. While the trend is not monotonic for fiber tips, the error for all four points probed remained within very reasonable accuracy (i.e., 0.25%). The numerical studies indicated that the sensitivity to the numerical integration of the constraint equation is the main factor leading to non-monotonic convergence. The integration rule selection formula introduced in Section 4.3 leads to highly accurate results, yet with some variation from monotonic convergence in some cases. The demonstrated errors are point-wise in contrast to the more traditional error characterization where the errors over the entire problem domain is averaged. We note that the highest errors within the model typically occurs at the fiber tips, which are directly reported in Fig. 8. The global error of the proposed approach is much more favorable compared to the reported point-wise values.

We also investigated the effect of fiber tip location on the local accuracy characteristics of the XFEM method. Figures 9 and 10 illustrate the accuracy characteristics of the XFEM model for cases in which the fiber tips lay within the elements or on element edges, respectively. In both cases we observed that the XFEM models display reasonable accuracy and follows the same trend as when fiber tips are on the nodes with a slightly higher errors. The accuracy of the model is higher when the fiber tip resides on the edges rather than within the element. The slight deviation from monotonic mesh convergence is attributed to the fact that the relative positions of the fiber tip for each mesh density is different leading to slightly different accuracy of the numerical integrations. For instance, if the fiber tip is too close to a node location, the sub elements formed in the Delaunay triangulation for numerical integration of the fully and partially enriched elements have very high aspect ratios. In all cases the accuracy of the XFEM model is in reasonable agreement with the reference finite element model. The point-wise comparison of the performance of XFEM models as a function of fiber tip location is summarized in Table 1 for three normalized mesh densities.

The XFEM method is known to exhibit sensitivity to the position of the enrichment functions with respect to the finite element mesh. The position sensitivity in the context of the present problem is investigated by considering the response of a fiber with fixed orientation and length that is swept across the problem domain. The accuracy of the model predictions is quantified as a function of the fiber relative position within the mesh. The angle and length of the fiber is 61^{o} to the horizontal and 1 mm, respectively. The sweep starts with the left fiber tip starting at 0.5 mm from the left edge and ends at 3.25 mm from the left edge of the domain. Simulations were conducted for each fiber position with a resolution of 0.1 mm. The errors at points C and D corresponding the bottom left and right corners of the domain remain consistently below 0.02%. The errors at the fiber tips tended to decrease slightly as it moved across the domain but clearly demonstrate the position sensitivity of the accuracy as illustrated in Fig. 11. The errors oscillate since the relative position of the fiber with respect the elements in the regular grid repeats as the fiber is moved an amount equal to the element size. The largest errors occur when the tips of the fibers are positioned at the center of an element. Figure 11 shows the absolute errors at the four points studied across the domain.

Random short fiber composite

In this section, we investigate the response of two-dimensional random short fiber composites. The matrix is taken to be portland cement with the elastic modulus of 14 GPa, Poisson's ratio of 0.3 and a domain of 100 mm by 100 mm. The cement matrix is reinforced in a planar fashion using carbon microfibers. The elastic moduli, length and diameter of the microfibers are 207 GPa, 7 mm ($\pm$ 1 mm) and 7 μm, respectively. Due to the high stiffness ratio between the reinforcement and matrix, we consider the deformation of the fibers to be rigid.

A set of volume elements with specified weight fractions of up to 0.15% are generated and subjected to uniform uniaxial stress to determine the effective properties of the composite material as a function of fiber weight fraction. The microstructures are generated to ensure that no element within the mesh is crossed by more than a single fiber. Figure 12 shows an example of the random short fibers in a domain. At each of the 6 different weight fractions studied, 20 microstructures are generated to characterize the variability of the effective modulus as a function of the fiber distribution properties. The variability of the effective modulus is due to two distinct factors: (a) the natural variability due to the random positioning of the fibers within the matrix in each realization; and (b) the effect of overall volume element size (i.e., statistical representativeness of the volume element). The effect of the second factor is minimized by choosing large enough representative volumes. This size of the volumes are determined as the smallest matrix volume beyond which the modulus variability does not significantly change. For a given weight fraction, preliminary simulations using different volume sizes were conducted. The modulus variability was found to be higher when the volume size is smaller. Beyond a threshold size, the variability of the modulus stabilizes. Similar simulations conducted at varying weight fractions showed that the threshold size for large weight fractions is bigger compared to small weight fractions. The representative volume size is therefore larger at higher fiber weight fractions.

Figure 13 illustrates the XFEM response of the random short fiber composite compared to the direct finite element method simulations performed with the commercial software package, Abaqus. The Young's Modulus of the random short fiber composite is plotted as a ratio with the initial Young's Modulus. At each weight fraction, 20 randomly generated microstructures are simulated using both the XFEM and the reference models. The results of the XFEM and the reference simulations are plotted including the mean value and standard deviation for each method. The elastic modulus tended to initially increase almost linearly and then started to level out with the increase of weight fraction. The XFEM results had variation due to the randomness of the fibers in the domain but were within 2% of the mean Abaqus results, which was slightly below the mean of the XFEM results for each weight fraction.

Conclusions

The formulation and implementation of an Extended Finite Element Method (XFEM) for random short fiber reinforced composite materials was proposed. A new enrichment function was used to incorporate the effect of random fiber inclusions within the XFEM framework and eliminated the need of using finite element meshes compliant with fiber inclusions. The motion of the fiber inclusions were modeled by constraining the deformation field along the domain of the fiber inclusions. Numerical integration procedures were provided for accurate evaluation of the system response for fiber tips that lay on arbitrary positions within the problem domain and for the rigid constraint of the fibers. The coupling of the XFEM method along with the new enrichment function and constraint equations formulated the elastic response of short fiber reinforced composites. The numerical examples verified the performance characteristics of the proposed model against the direct finite element method. The proposed approach accurately characterizes the elastic response of short fiber reinforced composites without the need for mesh compliance.

Several important advancements to the proposed model are under development. First, this manuscript provided the implementation details for 2-D problems only. While the proposed formulation can be extended to three-dimensions without conceptual difficulty, significant challenges are present in the computational implementation of the method in 3-D. Second is the incorporation of the failure processes present within the material. One key future development will be modeling the debonding process along the fiber-matrix interfaces. While cohesive zone models have been effective in numerical modeling of the debonding process along interfaces between distinct solid subdomains resolved with finite elements, incorporating the debonding process within the XFEM method and on sets of measure zero (i.e., fibers modeled as line elements within a volume) remains an open research question. Our near term research efforts will therefore focus on extending the proposed modeling approach to 3-D and account for failure processes.

Acknowledgements

The authors gratefully acknowledge the Vanderbilt University Discovery Grant Program for funding and support of this research.

References

Babuska, I. and Melenk, J. M. (1997). The partition of unity method. *Int. J. Numer. Meth. Engng.*, 40:727–758.

Belytschko, T. B., Gracie, R., and Ventura, G. (2009). A review of extended/generalized finite element methods for material modeling. *Modelling Simul. Mater. Sci. Eng.*, 17:043001.

Belytschko, T. B., Moes, N., Usui, S., and Parimi, C. (2001). Arbitrary discontinuities in finite elements. *Int. J. Numer. Meth. Engng.*, 50:993–1013.

Bohm, H. J., Eckschlager, A., and Han, W. (2002). Multi-inclusion unit cell models for metal matrix composites with randomly oriented discontinuous reinforcements. *Computational Materials Science*, 25:42–53.

Bordas, S. P. A., Rabczuk, T., Hung, N. X., Nguyen, V. P., Natarajan, S., Bog, T., Quan, D. M., and Hiep, N. V. (2010). Strain smoothing in fem and xfem. *Computers & Structures*, 88:1419–1443.

Bouaziz, A., Nait-Abdelaziz, M., Gloaguen, J. M., and Lefebvre, J. M. (2007). Micromechanical modelling and experimental investigation of random discontinuous glass fiber polymer–matrix composites. *Compos. Sci. Technol.*, 67:3278–3285.

Chen, L., Rabczuk, T., Bordas, S. P. A., Liu, G. R., Zeng, K. Y., and Kerfriden, P. (2012). Extended finite element method with edge-based strain smoothing (esm-xfem) for linear elastic crack growth. *Comput. Methods Appl. Mech. Engrg.*, 209-212:250–265.

Chessa, J., Wang, H., and T.Belytschko (2003). On the construction of blending elements for local partition of unity enriched finite elements. *Int. J. Numer. Meth. Engng.*, 57:1015–1038.

Chung, D. (2000). Cement reinforced with short carbon fibers: a multifunctional material. *Composites Part B: Engineering*, 31:511–526.

Chung, D. (2002). Composites get smart. *Materials Today*, 5:30–35.

Fries, T. (2008). A corrected xfem approximation without problems in blending elements. *Int. J. Numer. Meth. Engng.*, 75:503–532.

Fu, X. and Chung, D. D. L. (1996). Submicron carbon filament cement-matrix composites for electromagnetic interference shielding. *Cement and Concrete Research*, 26(10):1467–1472.

Hiriyur, B., Waisman, H., and Deodatis, G. (2011). Uncertainty quantification in homogenization of heterogeneous microstructures modeled by xfem. *Int. J. Numer. Meth. Engng.*, 88:257–278.

Huang, J. H. (2001). Some closed-form solutions for effective moduli of composites containing randomly oriented short fibers. *Mater. Sci. Eng. A*, 315:11–20.

Laborde, P., Pommier, J., Renard, Y., and Salaun, M. (2005). High-order extended finite element method for cracked domains. *Int. J. Numer. Meth. Engng.*, 64:354–381.

Li, V. (2003). On engineered cementitious composites (ecc) - a review of the material and its applications. *Journal of Advanced Concrete Technology*, 1:215–230.

Lusti, H. R., Hine, P. J., and Gusev, A. A. (2002). Direct numerical predictions for the elastic and thermoelastic properties of short fibre composites. *Compos. Sci. Technol.*, 62:1927–1934.

Moës, N., Cloirec, M., Cartraud, P., and Remacle, J.-F. (2003). A computational approach to handle complex microstructure geometries. *Comput. Methods Appl. Mech. Engrg.*, 192:3163–3177.

Moës, N., Dolbow, J., and Belytschko, T. (1999). A finite element method for crack growth without remeshing. *Int. J. Numer. Meth. Engng.*, 46:131–150.

Mohammadi, S. (2008). *Extended Finite Element Method for Fracture Analysis of Structures.* Blackwell, Oxford, UK.

Ponte-Castaneda, P. and Willis, J. R. (1995). The effect of spatial distribution on the effective behavior of composite materials and cracked media. *J. Mech. Phys. Solids*, 43:1919–1951.

Ravichandran, R., Venugopal, J. R., Sundarrajan, S., Mukherjee, S., Sridhar, R., and Ramakrishna, S. (2012). Minimally invasive injectable short nanofibers of poly(glycerol sebacate) for cardiac tissue engineering. *Nanotechnology*, 23:1–14.

Reza, F., Yamamuro, J. A., and Batson, G. B. (2004). Electrical resistance change in compact tension specimens of carbon fiber cement composites. *Cement and Concrete Composites*, 26:873–881.

Russel, W. B. (1973). On the effective moduli of composite materials: effect of fiber length and geometry at dilute concentrations. *Z. Angew. Math. Phys.*, 24.

Sukumar, N., N. Moes, B. M., and Belytschko, T. (2000). Extended finite element method for three-dimensional crack modelling. *Int. J. Numer. Meth. Engng.*, 48:1549–1570.

Tandon, G. P. and Weng, G. J. (1986). Average stress in the matrix and effective moduli of randomly oriented composites. *Compos. Sci. Technol.*, 27:111–132.

Location	Point A			Point B		
h/l	0.05	0.025	0.0125	0.05	0.025	0.0125
Tips at nodes	0.219%	0.085%	0.018%	0.079%	0.058%	0.015%
Tips at edges	1.099%	0.096%	0.140%	0.563%	0.165%	0.089%
Tips in element	1.459%	0.972%	0.358%	0.417%	0.463%	0.162%
Location	Point C			Point D		
h/l	0.05	0.025	0.0125	0.05	0.025	0.0125
Tips at nodes	0.095%	0.090%	0.025%	0.034%	0.032%	0.009%
Tips at edges	0.011%	0.006%	0.002%	0.010%	0.018%	0.012%
Tips in element	0.447%	0.172%	0.029%	0.592%	0.164%	0.140%

Table 1: Point wise absolute error comparison.

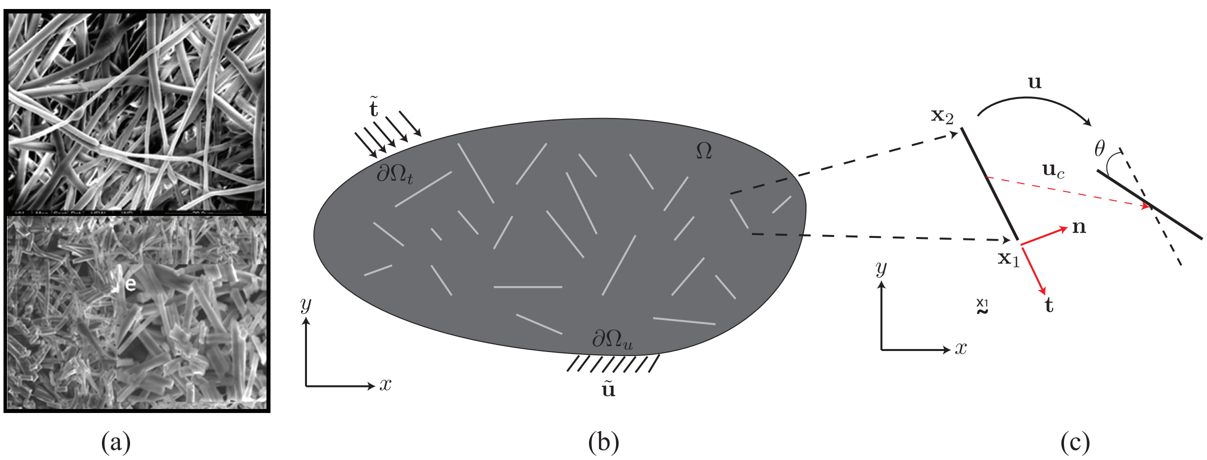

Figure 1: (a) Short fiber reinforced composite (from Ravichandran et al. (2012)); (b) domain of the short fiber reinforced composite; (c) short fiber kinematics.

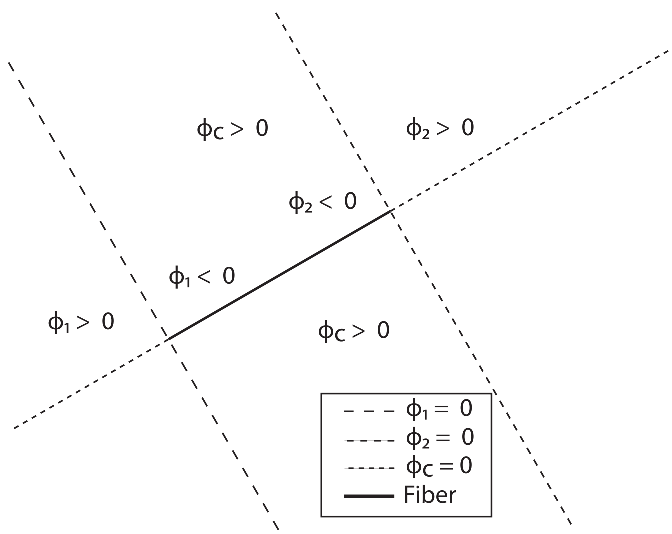

Figure 2: Level set functions of the enrichment.

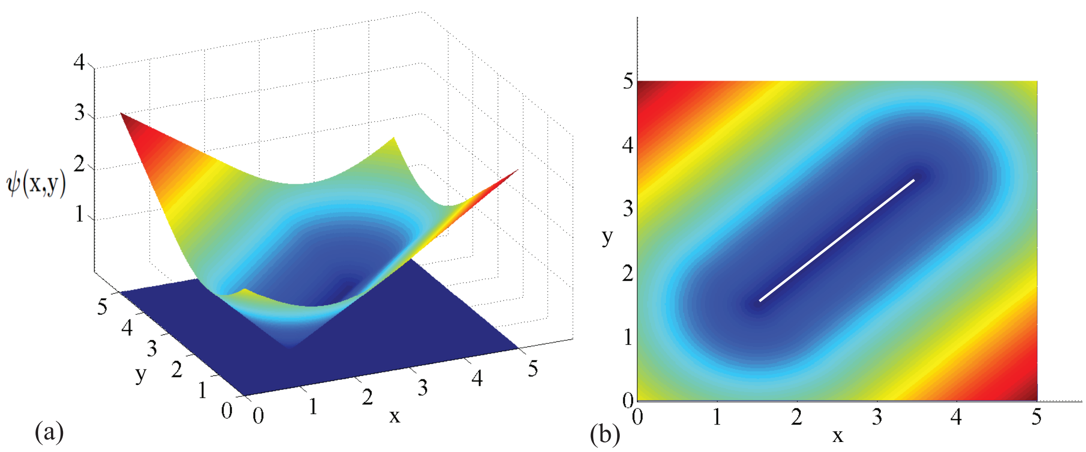

Figure 3: Short fiber inclusion enrichment function: (a) three dimensional view; (b) planar view (fiber is illustrated by the white line).

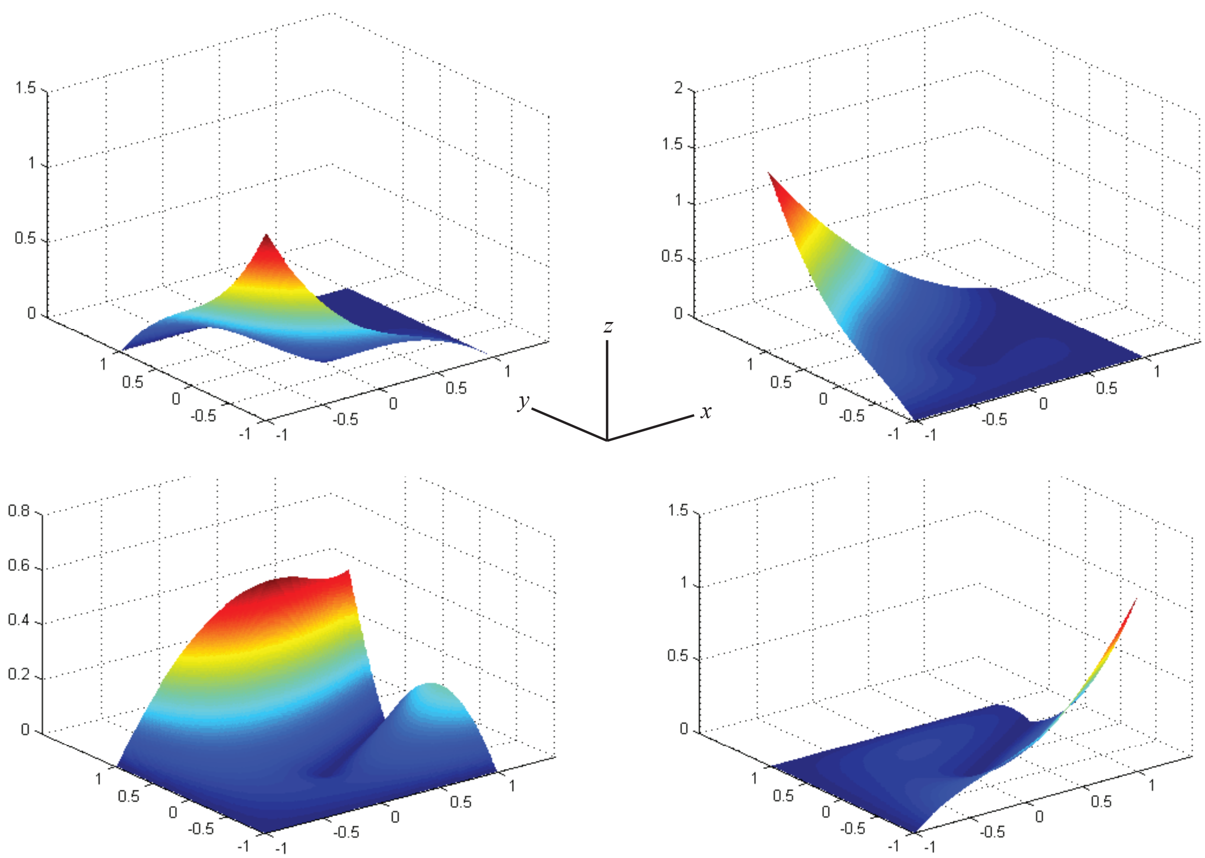

Figure 4: The nodal enrichments computed for a 2-D quadrilateral element. The fiber tip is within the element domain.

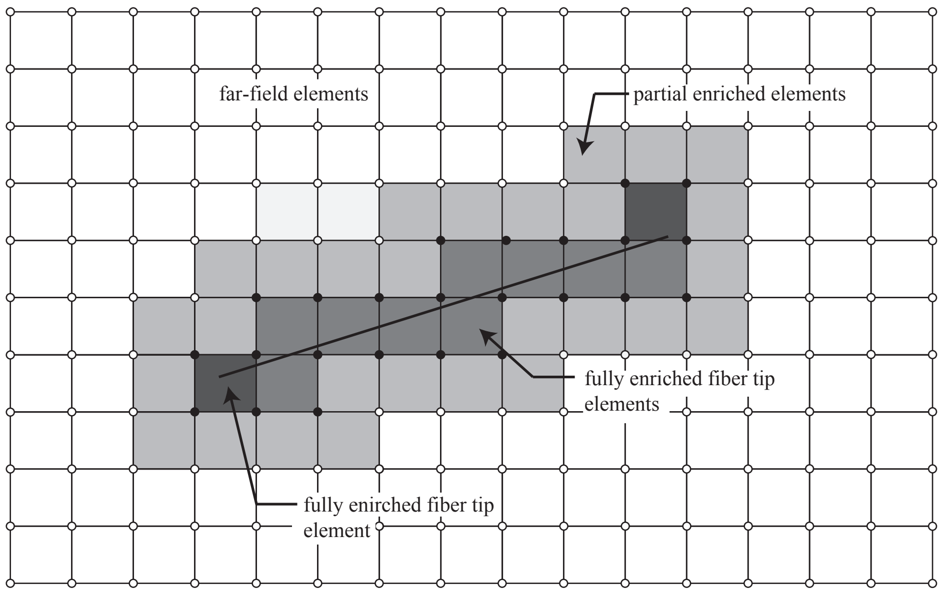

Figure 5: The decomposition of the problem domain into subdomains of far-field elements approximated by standard basis, partially and fully enriched elements.

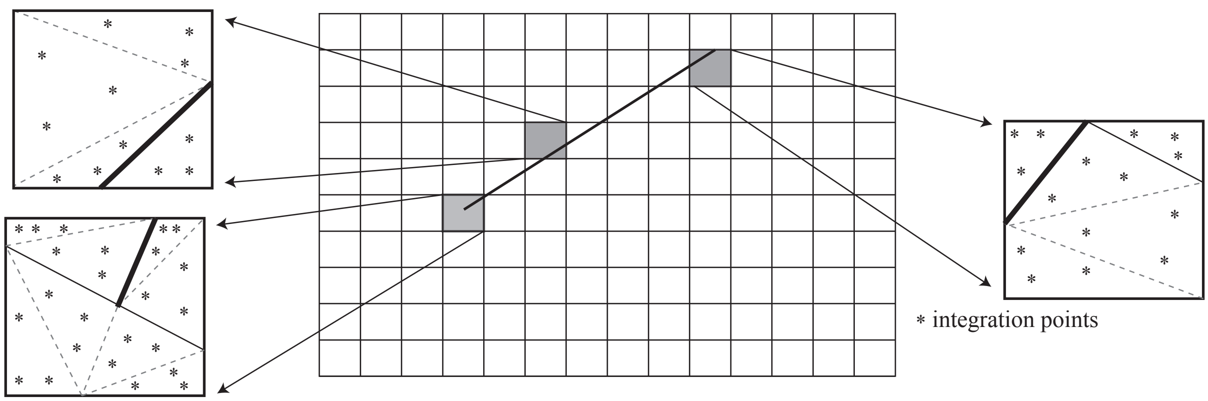

Figure 6: The schematic illustration of Delaunay triangulation and integration of fully enriched elements based on fiber tip positioning.

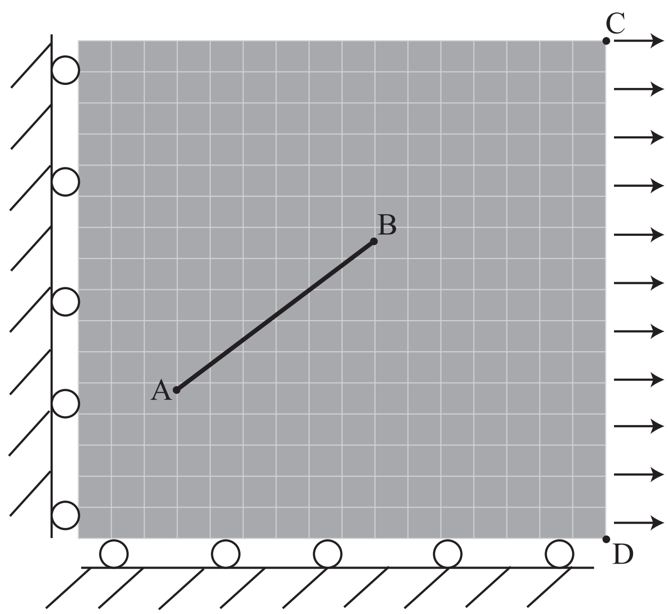

Figure 7: The geometry and boundary conditions of the single inclusion problem.

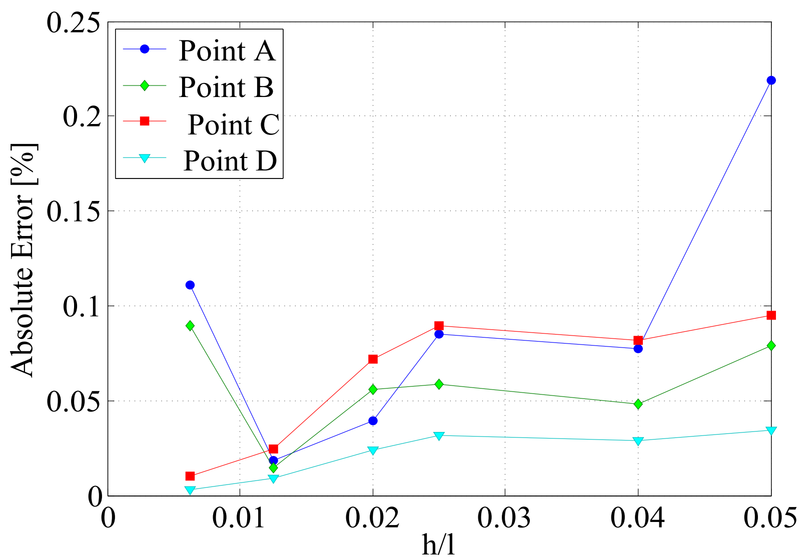

Figure 8: Error as a function of normalized mesh density when fiber tips are at mesh nodes.

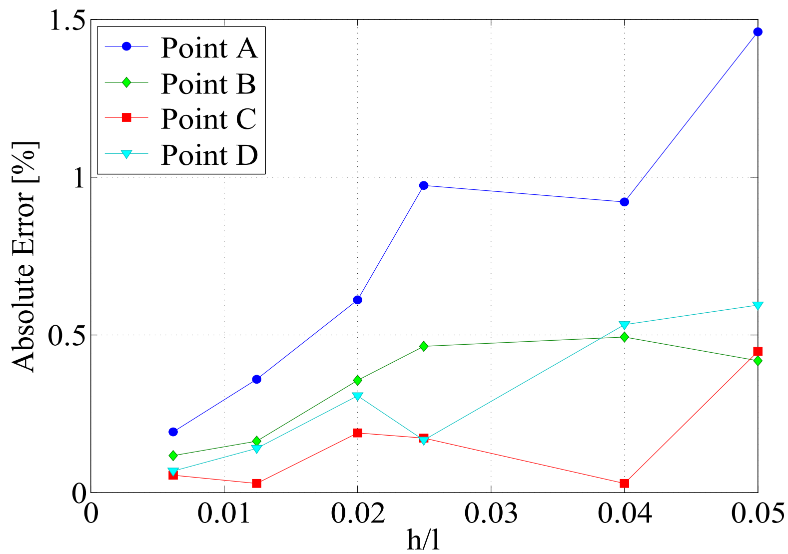

Figure 9: Error as a function of normalized mesh density when fiber tips in elements.

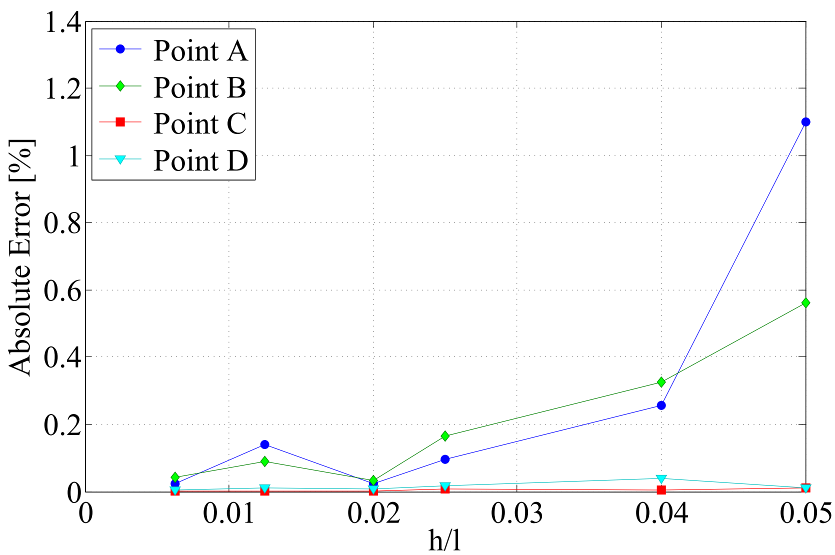

Figure 10: Error as a function of normalized mesh density when fiber tips are on element edges.

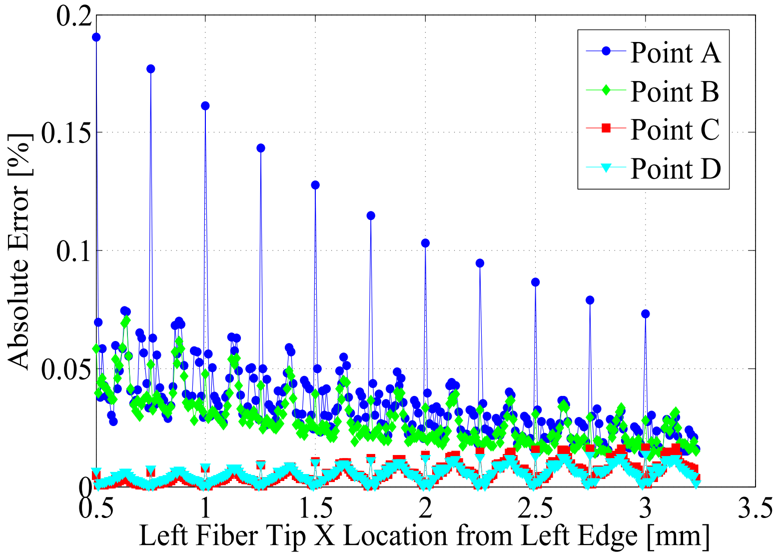

Figure 11: Error as a function of tip location across domain.

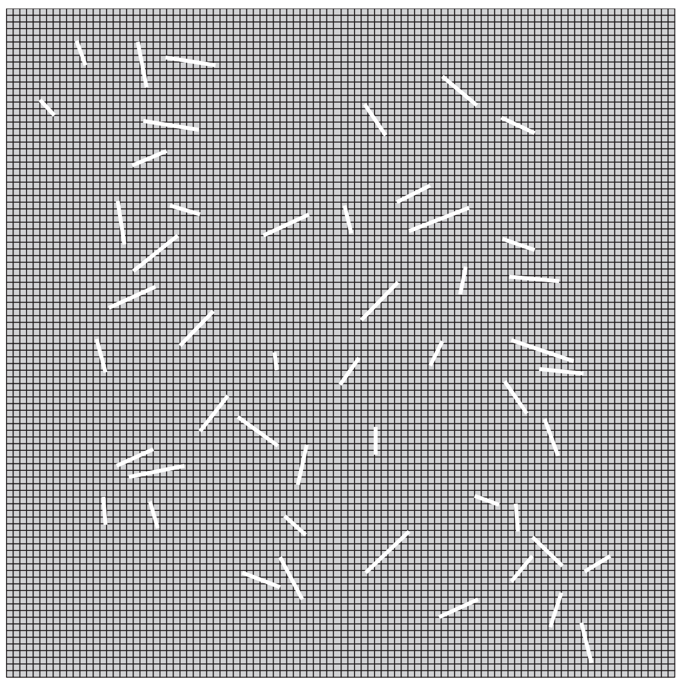

Figure 12: Random short fiber domain.

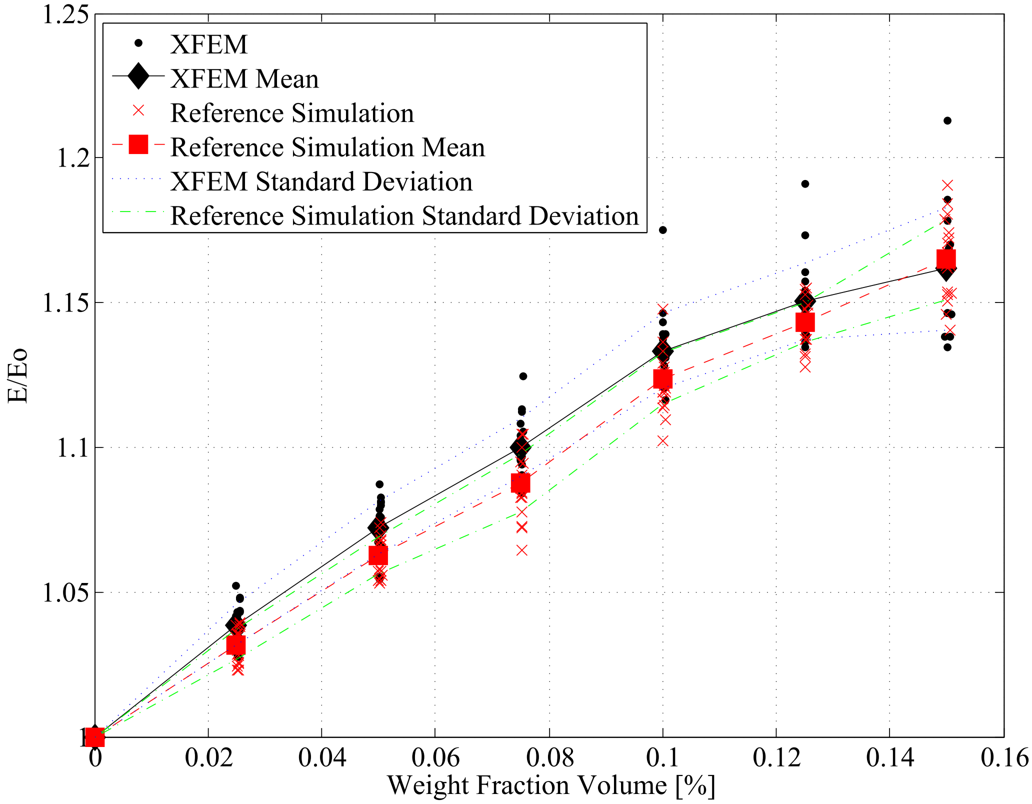

Figure 13: Elastic modulus ratio of random short fibers.